Available online at www.sciencedirect.com

ScienceDirect

Procedia Structural Integrity 3 (2017) 354–361

Structural Integrity Procedia

www.elsevier.com/locate/procedia

XXIV Italian Group of Fracture Conference, 1-3 March 2017, Urbino, Italy

A variational model for determining fracture modes in FRCM systems

Giovanni Lancioni [a]*, Jacopo Donnini[a], Valeria Corinaldesi[a]

[a]*Università Politecnica delle Marche, Engineering Faculty, Via Brecce Bianche, Ancona 60121, Italy*

Abstract

The bond strength at the yarn to matrix interface is one of the key factor affecting the FRCM mechanical behavior. The interaction between multi-filament yarn and cementitious matrix, governed by complex mechanisms, determines the behavior and failure mode of this composite system.
An experimental campaign comprising of 20 pull out tests on multifilament carbon yarns embedded in a cementitious matrix was carried out. Different bond lengths have been analyzed, equal to 20 and 50 mm. Failure modes observed were different depending on the bond length: slippage of the yarn for a bond length of 20 mm and failure of the external filaments when the bond length was increased to 50 mm. The maximum load recorded at fibers breakage was lower than the tensile strength of the yarn, confirming the fact that only the external filaments of the yarn are engaged in the load transfer mechanism and the effective area is only a portion of the total area.
This work aims to propose a variational model to reproduce the behavior and possible failure modes of multifilament carbon yarns embedded in a cementitious matrix. Smeared crack terms are incorporated into the energy functional of the model to account for possible fracture in the yarn and in the matrix, and for debonding at the yarn-matrix interface. The evolution problem is formulated as an incremental energy minimization problem, and discretized by finite elements. Numerical simulations are able to accurately describe the composite behaviours and to reproduce experimental results.

Peer-review under responsibility of the Scientific Committee of IGF Ex-Co.

Keywords: FRCM; interface; bond; yarn; variational modelling.

* Corresponding author.
E-mail address: g.lancioni@univpm.it

Copyright © 2017 The Authors. Published by Elsevier B.V. This is an open access article under the CC BY-NC-ND license (http://creativecommons.org/licenses/by-nc-nd/4.0/).
Peer-review under responsibility of the Scientific Committee of IGF Ex-Co.
10.1016/j.prostr.2017.04.031

1. Introduction

Fiber Reinforced Cementitious Matrix (FRCM) systems represent a valid alternative to Fiber Reinforced Polymer (FRP) as externally bonded reinforcement for masonry and RC structures (Nanni (2012)). The presence of an inorganic matrix offers numerous advantages such as better compatibility with substrate (both masonry or concrete), higher vapor permeability and fire resistance, more security for operator (Triantafillou et al. (2006)).
FRCM mechanical properties are strongly influenced by the ability of the inorganic matrix to impregnate dry fiber yarns: the level of penetration of the matrix within the filaments of the yarn characterizes the interfacial bond properties (Banholzer (2004)). The literature regarding FRCM composites is still very limited, and a fully exploitation of the stress-transfer mechanisms between multifilament yarns and matrix is not available. However, some studies showed that the interaction between filaments and matrix is characterized by different bond parameters. The bond between multifilament yarns and cementitious matrix has been studied by several authors Zhang et al. (2013), Namure (1989), Li (1997), Carozzi et al. (2016), by using different methods.
This work aims to investigate about the FRCM interface behaviour and failure mechanisms by means of pull-out tests on dry carbon yarns embedded in a cementitious matrix. To better understand the experimental results, a variational damage model has been developed and numerically implemented in a finite element code. The evolution of strain and damage in the system is determined by solving an incremental energy minimization problem, a powerful mathematical tool used in many variational problems (Del Piero et al. (2013), Lancioni (2015), Lancioni et al. (2015)). Non-local damage terms are incorporated into the energy functional of the model to account for possible cracks in the matrix and in the yarn, and a non-linear damage term accounts for possible debonding at the yarn-matrix interface. This latter term, proposed in Donnini et al. (2017), also allows to reproduce the bebonding observed in yarns coated with epoxy resins, not considered in the present paper, which typically exhibits long softening tails in the shear-stress versus sliding displacement curves. The two failure modes observed in pull-out experiments have been reproduced by numerical simulations: breakage of the yarn filaments at separation point between embedded and free length of the yarn, when large yarn bond lengths are considered, and debonding at the interface between yarn and matrix in the case of small yarn bond lengths. In this paper, experimental results are used first to properly calibrate some model parameters, and then to check the accuracy of numerical simulations.

2. Experimental investigation

An experimental campaign comprising of 20 pull out tests on carbon yarns embedded in a cementitious matrix was carried out. Tests were performed using a testing machine with a load bearing capacity of 5 kN. The FRCM material investigated is composed of a cementitious matrix and a dry carbon yarn. The mechanical properties of the matrix, fiber and yarn are reported in Table 1and Table 2.

Table 1. Material properties: mortar

Material	Compressive strength (MPa)	Splitting tensile strength (MPa)	Elastic modulus (GPa)	Unit weight (kg/m^3)	Yarn Poisson ratio ν_m
Cementitious Mortar	45	4.2	20	1320	0.2

Table 2. Material properties: fibers and yarn

Material	Tensile strength (MPa)	Elastic modulus (GPa)	Break elongation (%)	Reinforc. Area (A_f) (mm^2/cm)	Fabric weight (g/m^2)
Carbon fiber	4900	240	2	0.52	186
DRY Carbon yarn	1850	150	1.4		

The pull-out test was realized on a single dry carbon yarn embedded in a cementitious matrix for a length equal to 20 or 50 mm. The matrix is fixed at the top by a metallic frame anchored to the testing machine and the yarn is gripped and pulled in displacement control at 0.5 mm/min (Figure 1). The result of this test is a load f versus displacement s relation.

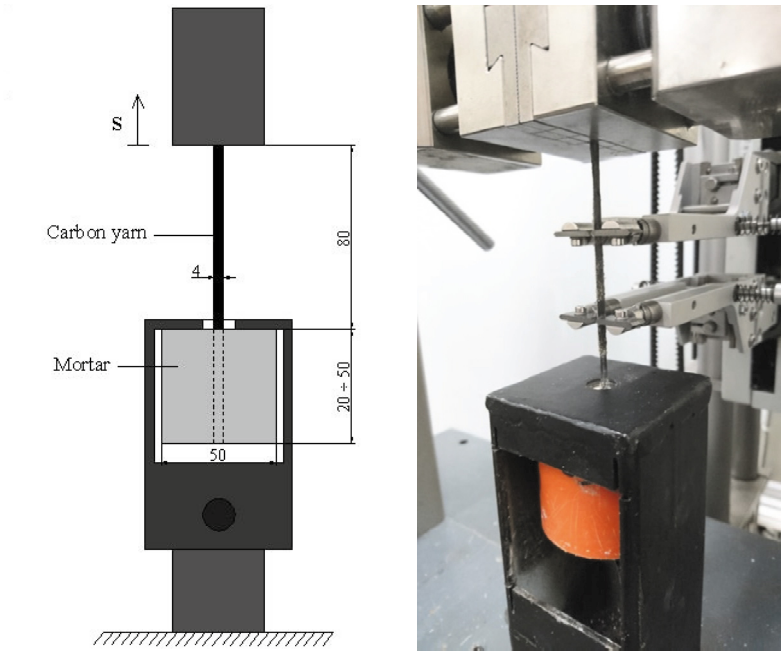

Fig. 1. Pull-out test set up

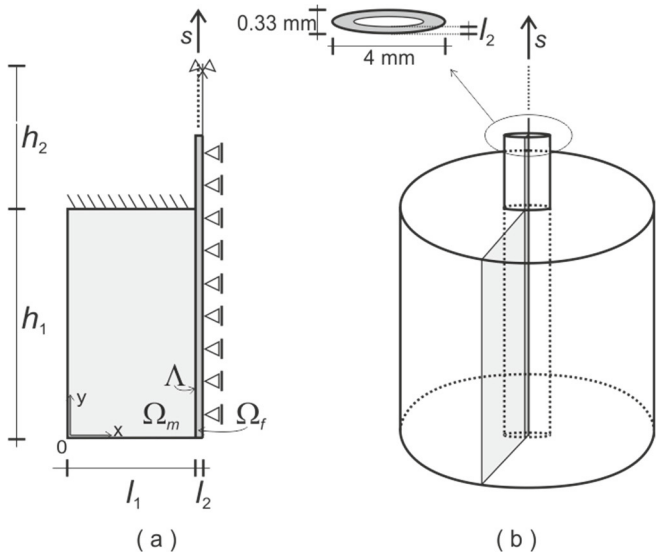

Fig. 2. (a) Pull-out test sample. (b) Two-dimensional geometry of simulations.

3. Fracture model

3.1. Geometrical scheme for pull-out test

The two-dimensional geometrical scheme considered in the numerical simulations is represented in Fig. 2(a). It is obtained from the three-dimensional sample of Fig. 2(b), by splitting the sample into two parts, along the shortest

axis of the yarn cross-section, and by considering only one-half of the resulting longitudinal section, for symmetry reasons (grey surface in Fig. 2(b)). In this section, we assume the hypothesis of plane strain state, which is reasonable since the yarn cross-section has a very elongated ellipsoidal shape.
The yarn is constituted by dry carbon filaments which can slide one over the other, and only an external ring sustains tensile loadings [2], as shown in Fig. 2(b). Thus we assign the thickness l_2=0.04 mm to the yarn domain, corresponding to the thickness of the yarn ring representing the effective yarn cross-section, which is 30 % of the total yarn cross-section area. Two different heights of the matrix cylinder are considered, i.e., h_1=20 mm or 50 mm. The cylinder radius is l_1=25 mm, and the length of the external yarn portion is h_2=80 mm.

3.2. Variational model

We refer to the geometrical scheme drawn in Fig. 2(a), with Ω_m the matrix domain, Ω_f the yarn domain, and Λ the matrix-yarn interface. The displacement s applied at the upper side of Ω_f monotonically increases from 0 to a final positive value. Body loads are neglected. For a given Cartesian coordinate system (O;x,y), the displacement field is $\mathbf{u}(\mathbf{x}) = [u(x,y), v(x,y)]^T$, and the damage field is $\alpha(\mathbf{x})$, which is equal to zero when the material is sound, and equal to 1 when it is totally damaged. Matrix and yarn are supposed to be brittle, and their energy is

$$\mathrm{E}(\mathbf{u},\alpha) = \int_\Omega (1-\alpha)^2 W(\nabla\mathbf{u})d\mathbf{x} + \int_\Omega d\left(\alpha + \frac{l^2}{2}(\nabla\alpha)^2\right)d\mathbf{x}, \tag{1}$$

where Ω stands indifferently for Ω_m or Ω_f. The first integral represents the elastic strain energy, with the elastic energy density

$$W = \frac{E}{2(1+\nu)}\left(sym^2\nabla\mathbf{u} + \frac{\nu}{(1-2\nu)}tr\nabla\mathbf{u}^2\right), \tag{2}$$

of linearly elastic isotropic materials, depending on the Young's modulus E and the Poisson's ratio ν. Values assigned to matrix and yarn are E_m=34500 MPa, ν_m=0.2, and E_f=240000 MPa, ν_f=0.3, respectively. Young's modulus of single filament is assigned to the yarn domain, because only few are engaged in the load transfer mechanism from yarn to matrix.
The second integral in (1) represents the damage energy, and it is sum of a local linear term and a quadratic non-local gradient term. This energy is proper of materials which exhibits an initial elastic behaviour, followed by brittle failure. Parameter d is related to the maximum tensile stress σ_e attained in the elastic phase, and to the Young's modulus E by the formula $d = \sigma_e^2 / E$. Parameter l represents a material internal length, related to the width of the damage localization band B by the formula $l = B/(2\sqrt{2})$. These relations are determined in Pham et al. (2011) by solving the minimum problem associated to the functional (3) in the one-dimensional setting of a tensile test. For the matrix, we assign $\sigma_{e,m}$=6.2 MPa, and B_m=5mm, which is 2-3 times the size of the largest aggregate. For the yarn, we assume $\sigma_{e,f}$=1400 MPa, which is 75% of the yarn tensile strength to account for possible experimental misalignments, and B_f=1 mm.
A distribution of damageable elastic springs are assumed at the matrix-yarn interface Λ, whose energy is

$$\mathsf{E}_s(\boldsymbol{\delta},\alpha) = \int_0^{h_1} (1-\alpha)^2 \frac{1}{2}\mathbf{K}\boldsymbol{\delta}\cdot\boldsymbol{\delta}dy + \int_0^{h_1} \frac{a}{q}((1-\alpha)^{-q} - 1)dy\,. \tag{3}$$

It depends on the displacement jump at the interface $\boldsymbol{\delta}(y) = [\delta_x(y), \delta_y(y)]^T = \Delta\mathbf{u}$, with $\Delta\mathbf{u}$ the relative displacement yarn-matrix, and on the interface damage $\alpha(y)$, with $y \in (0,h)$. As in (1), the first integral represents the elastic energy, where the elastic tensor is $\mathbf{K} = k\mathbf{I}$, with $\mathbf{I}$ the identity tensor, and k the elastic coefficient of the

springs in the normal and tangential directions. We assume k=5 N/mm^3. The second integral represents the damage energy, which is a power function of α. The non-local term depending on $\nabla\alpha$, considered in (1), is neglected, and, as a result, α can localize in single points of the interface.
To characterize the coefficients a and q in the damage energy, we determine the equilibrium relations at the interface by requiring the first variation of (3) to be non-negative. Following a standard variational procedure, we obtain the equilibrium relations

$$\tau = (1-\alpha)^2 k\delta_y, \qquad -(1-\alpha)k\delta_y^2 + a(1-\alpha)^{-(q+1)} \geq 0\,. \tag{4}$$

The first equation is the linear shear stress-sliding displacement relation due to the springs, and the second relation represents the damage criterion. The damage can evolve, when $(4)_2$ is satisfied as an equality, and it cannot, if $(4)_2$ is a strict inequality. In a process of increasing τ, starting from an unstressed undamaged initial configuration, $(4)_2$ is strictly satisfied for $\alpha = 0$ and $\tau < \tau_e = \sqrt{ak}$. For $0 < \tau \leq \tau_e$, the evolution is purely elastic, and, for $\tau > \tau_e$, damage forms and evolves. Parameter a is calibrated by using the relation $a = \tau_e^2 / k$, where τ_e=1.7 MPa, and k=5 N/mm^3. In the damage phase $\tau > \tau_e$, $(4)_2$ is satisfied as an equality. Thus from (4) we obtain the shear stress-sliding displacement relation $\tau/\tau_e = (\delta/\delta_e)^{\frac{q-2}{q+2}}$, with $\delta_e = \tau_e / k$, whose graphs are plotted in Fig. 3 for different values of q. Notice that q controls the slope of the post-elastic branch. The damage regime is stress-hardening if q>2, stress softening if -2<q<2, and brittle if q=-2. Since dry yarns exhibit brittle slippage in experiments, we set q=-2. Values of q larger than -2 are considered in Donnini et. al. (2017) for yarns impregnated with resins, whose response curves are distinguished by long softening tails. Values of τ_e and k are taken from experiments on DRY_20, where τ and δ_y can be assumed homogeneous.

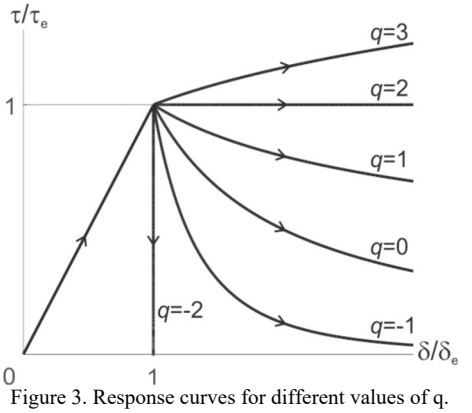

Figure 3. Response curves for different values of q.

The internal energy of the system is sum of the yarn and matrix energies of the form (1), and of the interface energy (3)

$$\mathrm{E}(\mathbf{u},\alpha) = \mathrm{E}_f(\mathbf{u},\alpha) + \mathrm{E}_m(\mathbf{u},\alpha) + \mathrm{E}_s(\boldsymbol{\delta}(\mathbf{u}),\alpha)\,, \tag{12}$$

which coincides with the total energy of the system, since volume and surface forces are null.
The evolution of $\mathbf{u}$ and α, for increasing s, is determined by means of incremental energy minimization. The displacement s is increased through finite steps, and within each step, $\mathbf{u}$ and α are supposed to be linear functions of s, $\mathbf{u}(s+\delta s) = \mathbf{u}(s) + \frac{d\mathbf{u}(s)}{ds}\delta s$, $\alpha(s+\delta s) = \alpha(s) + \frac{d\alpha(s)}{ds}\delta s$, and the energy $\mathrm{E}(\mathbf{u},\alpha)$ is developed up to the second order $\mathrm{E}(\mathbf{u}(s+\delta s),\alpha(s+\delta s)) = \mathrm{E}(\mathbf{u}(s),\alpha(s)) + s\frac{d\mathrm{E}}{ds}(\mathbf{u}(s),\alpha(s)) + \frac{1}{2}s^2\frac{d^2\mathrm{E}}{ds^2}(\mathbf{u}(s),\alpha(s))$.

The rates pair $\left(d\mathbf{u}(s)/ds,\ d\alpha(s)/ds\right)$ is determined by minimizing the above functional, under the constrain $d\alpha(s)/ds \geq 0$. A finite element code has been developed in MATLAB which implements an alternate iterative minimization procedure, consisting in minimizing the energy functional with respect to the two unknown fields separately.

4. Experimental and numerical results

Results of pull out tests are reported in Table 3 for the different geometries tested. The average maximum load f_{max} evaluated on 5 specimens for each type of geometry and the relative displacement s_{max} are reported. The maximum shear stress $\tau_{e,max}$ at the interface is calculated as $\tau_{e,max} = f_{max} / (h_1 \cdot p)$, with p the perimeter of the yarn equal to 8 mm, and the elastic modulus $k=\tau_{e,max}/\delta_{max}$, with $\delta_{max}=s_{max}-\sigma_{max}\cdot h_2/E_f$ the displacement of the yarn section of coordinate h_1. The failure mode observed is different for the two geometries tested: slippage of the yarn within the matrix for h_1 = 20 mm, breakage of the external filaments of the yarn (active filaments) for h_1 = 50 mm.

Table 3. Experimental results of pull-out test.

Carbon yarn		Bond length h_1 (mm)	Max Load f_{max} (N)	Stress in the yarn s_{max} (MPa)	s_{max} (mm)	□$_{max}$ □*mm)*	$\tau_{e,max}$ (MPa)	k (N/mm^3)	Failure mode
DRY_20	Average	20	262	252	0.63	0.56	1.64	2.93	Slippage
	CoV (%)	-	*14.2*	*14.2*	*11.5*	*11.5*	*14.2*	*14.3*	
DRY_50	Average	50	479	460	0.87	0.72	1.20	1.67	Fibers' breakage
	CoV (%)	-	*6.03*	*6.03*	*15.1*	*15.1*	*6.03*	*13.2*	

Fig. 4. Failure modes observed in pull-out tests: (a) slippage;(b) fibers breakage.

Experimental results showed an increase of the maximum load by increasing the bond length. The shear stress calculated as constant stress at the yarn-matrix interface $\tau_{e,max}$ decreased by increasing the bond length. The stress in the yarn section increased by increasing the bond length up to 460 MPa for h_1=50 mm. The failure of the yarn for a tensile stress lower than the ultimate tensile capacity of the yarn confirmed the fact that only a portion of the yarn (external filaments) is carrying the load (about 30% of the total yarn's area).

Two numerical simulations are performed, by considering the two different sample geometries DRY_20 (h_1=20 mm) and DRY_50 (h_1=50 mm). Curves of the force f applied to yarn versus the displacement s registered at the yarn upper extremity are plotted in Fig. 5 (solid line) and compared to the experimental curves (dotted line). Simulations accurately estimates the maximum force reached right before failure occurrence: 250 N for h_1=20 mm, and 475 N

for h_1=50 mm. Even the slope of the curves in the initial elastic phase is satisfactorily captured. Simulations account for brittle failure, thus they do not reproduce the short softening tails observed in experiments, which correspond to phases of progressive breaking of the external filaments before failure. However, the final failure modes are perfectly caught: the 20 mm height sample fails by slippage of the yarn with respect to the matrix, and the 50 mm height sample collapses by break of the external filaments of the yarn.

Slippage mechanisms is described in Fig. 6(a), where four different profiles of the damage parameter α at the yarn-matrix interface, determined at steps of the evolution process across failure, are drawn. Numbers are used to label the sequence of profiles. Profile 1, with α=0 in the whole interface, corresponds to sound interface. Yarn starts to separate at the upper extremity of the interface, and detachment progressively evolves downward, as shown by profiles 2 and 3. For this two profiles, the front of the debonded (totally damaged) zone is at about y=18 mm and y=14 mm. As the front has reached the coordinate y=13 mm, the rest of the interface brutally breaks, leading to the slippage of the yarn from the matrix. This situation is described by profile 4, where α=1 all over the interface.

The sample DRY_50 experiences a totally different failure mechanism. Indeed it undergoes breakage of the yarn at the point of separation between the embedded part and the free part. The profile of α is plotted in Fig. 6(b). Fracture forms in the narrow zone of coordinate y=50 mm, where α jumps to 1.

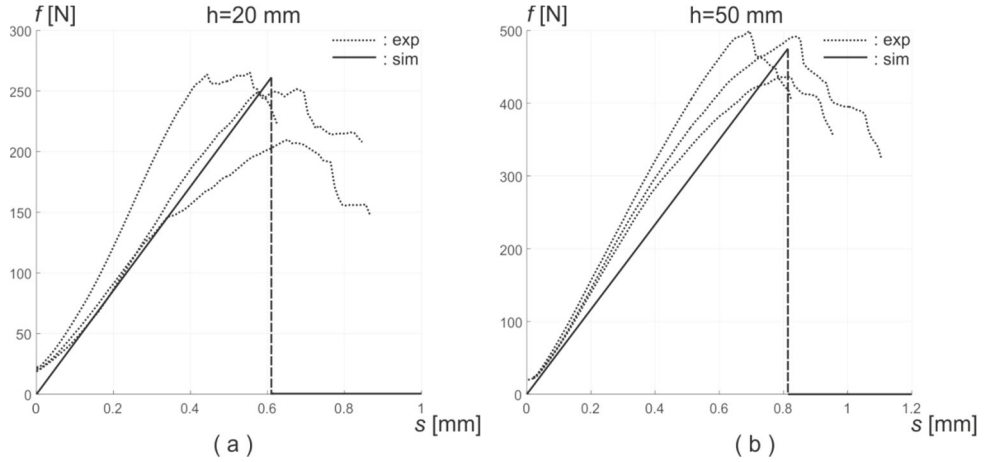

Figure 5. Experimental (dotted line) and numerical (solid line) force-displacement curves for specimens height h=20 mm (a) and h=50 mm (b).

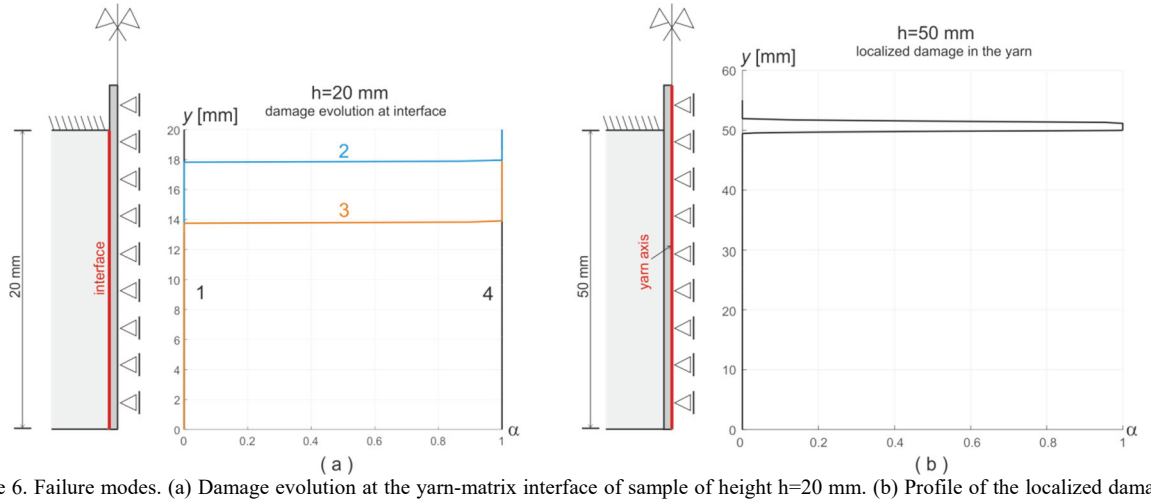

Figure 6. Failure modes. (a) Damage evolution at the yarn-matrix interface of sample of height h=20 mm. (b) Profile of the localized damage in the yarn axis of sample of height h=50 mm.

Conclusions

- Experimental and numerical results confirmed that in case of FRCM systems reinforced with dry carbon yarns only the external filaments of the yarn directly in contact with the matrix are able to carry the tensile load. The area of the yarn that is subject to tensile stress during the pull-out test, which can be defined as a set of 'active filaments' was evaluated as 30% of the total area from experimental investigations. The area of this thin outer ring of filaments was confirmed by numerical simulations.
- Two different failure modes were detected during pull-out tests, depending on the bond length of the yarn within the matrix. The yarn slips within the matrix for a bond length h_1=20 mm, while the system fails due to breakage of external filaments of the yarn if h_1=50 mm.
- The numerical model is able to catch the two different failure modes depending on the specimen geometry and to correctly simulate the pull-out behaviour of dry carbon yarns embedded in a cementitious matrix.

References

Banholzer, B., 2004. Bond behavior of multi-filament yarn embedded in a cementitious matrix, Ph.D. thesis, Rheinisch-Westfälische Technische Hochschule (RETH) Aachen Univ., Aachen, Germany.

Carozzi F.G., Colombi P., Fava G., Poggi C., 2016. A cohesive interface crack model for the matrix-textile debonding in FRCM composites. Composite Structures, 143, 230-241.

Del Piero, G., Lancioni, G., March, R., 2013. A diffuse cohesive energy approach to fracture and plasticity: the one-dimensional case. J. of Mechanics of Materials and Structures, 8(2-4), 109-151.

Donnini J., Corinaldesi V., Nanni A., 2016. Mechanical properties of FRCM using carbon fabrics with different coating treatments. Composites Part B: Engineering, 88, 220-228.

Donnini, J., De Caso y Basalo, F., Corinaldesi, V., Lancioni, G., Nanni, A., 2017. Fabric-reinforced cementitious matrix behavior at high-temperature: Experimental and numerical results. Composites Part B 108, 108-121.

Lancioni, G., 2015. Modeling the response of tensile steel bars by means of incremental energy minimization, J. Elast., 121(1), 25-54.

Lancioni, G., Yalcinkaya, T., Cocks, A., 2015. Energy-based non-local plasticity models for deformation patterning, localization and fracture. Proceedings of the Royal Society A, 471, 20150275.

Li V.C., Stang H., 1997. Interface property characterization and strengthening mechanics in fiber reinforced cement based composites. J. Advanced cement based materials, 6(1), 1-20.

Namure G., Naaman A.E., 1989. Bond stress model for fiber reinforced concrete based on bond stress-slip relationship. ACI Material Journal, 86(1), 45-47.

Nanni A., 2012. FRCM strengthening e a new tool in the concrete and masonry repair toolbox, Concrete International, 34.

Pham, K., Amor, H., Marigo, J.J., Maurini, C., 2011. Gradient damage models and their use to approximate brittle fracture. Int. J. Damage Mech. 20, 618-652.

Triantafillou T.C., Papanicolaou C.G., 2006. Shear strengthening of reinforced concrete members with textile reinforced mortar (TRM) jackets. Materials and Structures, 39(1), 93–103.

Zhang X.B., Aljewifi H., Li J., 2014. Failure mechanism investigation of continuous fibre reinforced cementitious composites by pull-out behaviour analysis. Procedia Material Science, 3, 1377-1382.